Ferromagnetic, Folded Electrode Composite as a Soft Interface to the Skin for Long-Term Electrophysiological Recording

*Kyung-In Jang, Han Na Jung, Jung Woo Lee, Sheng Xu, Yu Hao Liu, Yinji Ma, Jae-Woong Jeong, Young Min Song, Jeonghyun Kim, Bong Hoon Kim, Anthony Banks, Jean Won Kwak, Yiyuan Yang, Dawei Shi, Zijun Wei, Xue Feng, Ungyu Paik, Yonggang Huang, Roozbeh Ghaffari, and John A. Rogers**

A class of ferromagnetic, folded, soft composite material for skin-interfaced electrodes with releasable interfaces to stretchable, wireless electronic measurement systems is introduced. These electrodes establish intimate, adhesive contacts to the skin, in dimensionally stable formats compatible with multiple days of continuous operation, with several key advantages over conventional hydrogel-based alternatives. The reported studies focus on aspects ranging from ferromagnetic and mechanical behavior of the materials systems, to electrical properties associated with their skin interface, to system-level integration for advanced electrophysiological monitoring applications. The work combines experimental measurement and theoretical modeling to establish the key design considerations. These concepts have potential uses across a diverse set of skin-integrated electronic technologies.

1. Introduction

Recent advances in materials for soft, dry electrodes and their demonstrated use in transcutaneous recording of electrophysiological signals suggest opportunities for continuous collection of data of relevance to healthcare and non-healthcare related applications alike.[1–9] For long-term use (i.e., several days) and minimized irritation at the skin interface in forms that provide for natural motions of the skin and body, an ideal electrode design should enable 1) conformal and robust contact to the skin, in a low-modulus design to eliminate mechanically induced discomfort and time-dependent effects associated with variation in hydration level,[10–12] 2) mounting[7,13,14] on curvilinear surfaces of any region of the body,[15] and 3) direct integration with advanced wireless electronics for data collection and communication.[16] The most widely adopted solution relies on conductive hydrogels, whose attractive features include low elastic moduli, biocompatible materials options, and low interface impedances. Typically, the hydrogel contacts the skin on one side and a solid metal recording electrode on the other.[17,18] A key disadvantage is that the cross-linked hydrophilic polymer networks of the hydrogel can undergo dramatic dimensional changes when exposed to biofluids (e.g., sweat-induced swelling) or when

Prof. K.-I. Jang, H. N. Jung, Dr. J. W. Lee, Y. H. Liu, Dr. J. Kim, Dr. B. H. Kim, A. Banks, J. W. Kwak, Y. Yang, D. Shi, Z. Wei, Prof. J. A. Rogers
Department of Materials Science and Engineering
Frederick Seitz Materials Research Laboratory
University of Illinois at Urbana-Champaign
Urbana, IL 61801, USA
E-mail: jrogers@illinois.edu

Prof. K.-I. Jang
Department of Robotics Engineering
Daegu Gyeongbuk Institute of Science and Technology (DGIST)
Daegu 42988, Korea

Dr. J. W. Lee, Dr. J. Kim, Prof. U. Paik
Department of Material Science and Engineering
Department of Energy Engineering
Hanyang University
Seoul 133–791, Republic of Korea

Prof. S. Xu
Department of NanoEngineering
University of California at San Diego
La Jolla, CA 92093, USA

DOI: 10.1002/adfm.201603146

Dr. Y. Ma, Prof. X. Feng
Department of Engineering Mechanics
Center for Mechanics and Materials
Tsinghua University
Beijing 100084, China

Dr. Y. Ma, Prof. Y. Huang
Department of Civil and Environmental Engineering
Mechanical Engineering
Materials Science and Engineering
Northwestern University
Evanston, IL 60208, USA

Prof. J.-W. Jeong
Department of Electrical
Computer and Energy Engineering
University of Colorado
Boulder, CO 80309, USA

Prof. Y. M. Song
School of Electrical Engineering and Computer Science
Gwangju Institute of Science and Technology
Gwangju 61005, Republic of Korea

Dr. R. Ghaffari
MC10 Inc
Cambridge, MA 02140, USA

© 2016 WILEY-VCH Verlag GmbH & Co. KGaA, Weinheim

exposed to air (e.g., drying-induced shrinkage). More recent alternatives involve dry, but soft and tacky, materials in which direct contact and/or capacitive coupling occurs between a conducting filamentary metal mesh supported by an ultralow modulus elastomer support. This composite structure can conform to the skin and accommodate natural motions, with an elastic response to strains up to several tens of percent and moduli that are substantially lower than those of the skin itself, in forms that are dimensionally stable when exposed to biofluids and air.[7,16] Reversible integration with measurement systems requires, however, interconnects that are often cumbersome and fragile. Related approaches use nanomaterials (silver nanowires, graphene flakes, carbon nanotubes, etc.) coated on and/or embedded throughout the elastomer.[19–24] These options offer many attractive features, but precise dimensional control over the electrode geometries and interconnects can be difficult to achieve using existing manufacturing methods, and via connections for front to back side integration require specialized designs. Also, in most cases, the constituent nanomaterials are not commonly found in conventional electronics technologies.

Here, we present materials, integration strategies, and wireless electrophysiological recording demonstrations of an electrode structure that provides some key advantages over alternatives. The designs involve soft, composite layouts with embedded magnetic materials and a folded configuration. The result is a dry, long-lived interface to the skin, with reversible magnetic coupling to a separate measurement platform as a means to facilitate replacement, cleaning, and re-use. Systematic studies of the materials, the mechanical properties, the contact impedances to the skin establish the fundamental aspects of this materials technology. Demonstrations in continuous wireless EEG, EMG, ECG, and EOG recordings over several days establish the utility in practical applications.

2. Results and Discussion

Figure 1 presents a schematic diagram that shows a representative ferromagnetic, folded composite structure resting on a thin permanent magnet (NdFeB). The electrode incorporates a thin, filamentary serpentine wire mesh (yellow) that bonds to and wraps around a soft ferromagnetic core (black) via a thin, tacky elastomer adhesive shell (gray). The mesh serves as the recording interface (direct or capacitive, depending on the absence or presence of a dielectric overcoat on the metal) and adopts a lithographically defined network design to allow biaxial stretchability. The exposed regions of the low-modulus adhesive/ferromagnetic bi-layer provide adherent interfaces to the skin, with sufficient strength to maintain robust conformal contact under natural deformations associated with limb movements and muscle contractions. This contact prevents relative movement between the electrodes and the skin, thereby minimizing noise from motion artifacts. On the other side, the mesh electrically couples to a thin permanent magnet via a magnetic force of attraction that exceeds the strength of adhesion of the other side to the skin. The magnet also provides, on its back side, a permanent electrical bond to the recording hardware.

Figure 1b shows a sequence of fabrication steps. As described in the Experimental Section, the mesh electrodes consist of filamentary traces with widths of 100 μm and thicknesses of 1–2 μm (200 nm Au/10 nm Cr/1.2 μm polyimide for direct contact; 1.2 μm polyimide/200 nm Au/10 nm Cr/1.2 μm polyimide for capacitive contact). Fabrication involves photolithographic patterning of metals deposited by electron beam evaporation on a sacrificial layer of polymethylmethacrylate (PMMA, 1 μm). Immersing the sample into acetone for 1 h allows retrieval of the mesh onto a water soluble tape. Spin coating and thermally curing a tacky, ultralow modulus formulation of a silicone polymer (*Silbione* Firm Gel, Bluestar Silicones, France, $E \approx 20$ kPa) and a soft ferromagnetic composite formed by mixing uncured polymer with carbonyl iron (CI) powder (Sigma–Aldrich, USA, diameter ≈ 2 μm), as shown in **Figure 2**, forms a bilayer on the exposed surface of the mesh. The spherical iron particles of the CI powder randomly mix and disperse in the silicone polymer matrix. The particles have varying numbers of concentric layers of α-iron between which cementite (Fe_3C) stabilizes the structure.[25] The onion-like structure of the particles prevents the displacement of domain boundaries under an applied magnetic field. A result is that the magnetic hysteresis losses are very low.[26] As previously reported,[27] CI particle-filled siloxane elastomers involve physical embedding of the particles without significant chemical interactions. The resulting composite maintains its magnetic properties up to temperatures of 150 °C, where amorphous layers of cementite prevent the crystalline phase of α-iron from oxidation.[25] Since the maximum temperature of the fabrication process outlined above is 70 °C, the CI particles retain their magnetic permeability.

As shown in Figure 1b, partially curing the polymers, folding the structure in half, completing the curing process and then dissolving the water soluble tape (immersion in water for 1 h) yields stretchable magnetic electrodes. Figure 1c,d shows an optical image of a sample and a scanning electron microscope image of the folded region.

In use, as shown in Figure 2a, the electrode is in conformal contact with the skin on one side and with a thin magnet bonded to a wireless data acquisition and transmission system on the other. This configuration provides a mechanically compliant, electrically conductive channel, via the folded mesh, between the skin and the wireless system through the magnet. The middle layer, consisting of CI particles in a soft adhesive, silicone matrix, is magnetic and non-conductive.[28] Because the magnetic force exceeds the adhesion force, the system can be peeled away from the skin without delaminating the electrode from the wireless system. At the same time, the magnetic coupling allows reversible release of the electrode for cleaning or replacement. Figure 2b shows that the ferromagnetic particles in the elastomer matrix are nearly spherical in shape, with diameters between 1 and 3 μm and a mean of ≈2 μm. As plotted in Figure 2c, the magnetization curves obtained using a SQUID magnetometer indicate that the magnetization density rapidly increases with the strength of the external magnetic field, and then saturates at 2.2 T when the field strength reaches at 600 kA m^{-1}. Under the action of an external magnetic field, each particle embedded in the elastomer can be magnetized to form a magnetic dipole. The resulting magnetization is further increased by the local magnetic fields exerted by surrounding

© 2016 WILEY-VCH Verlag GmbH & Co. KGaA, Weinheim

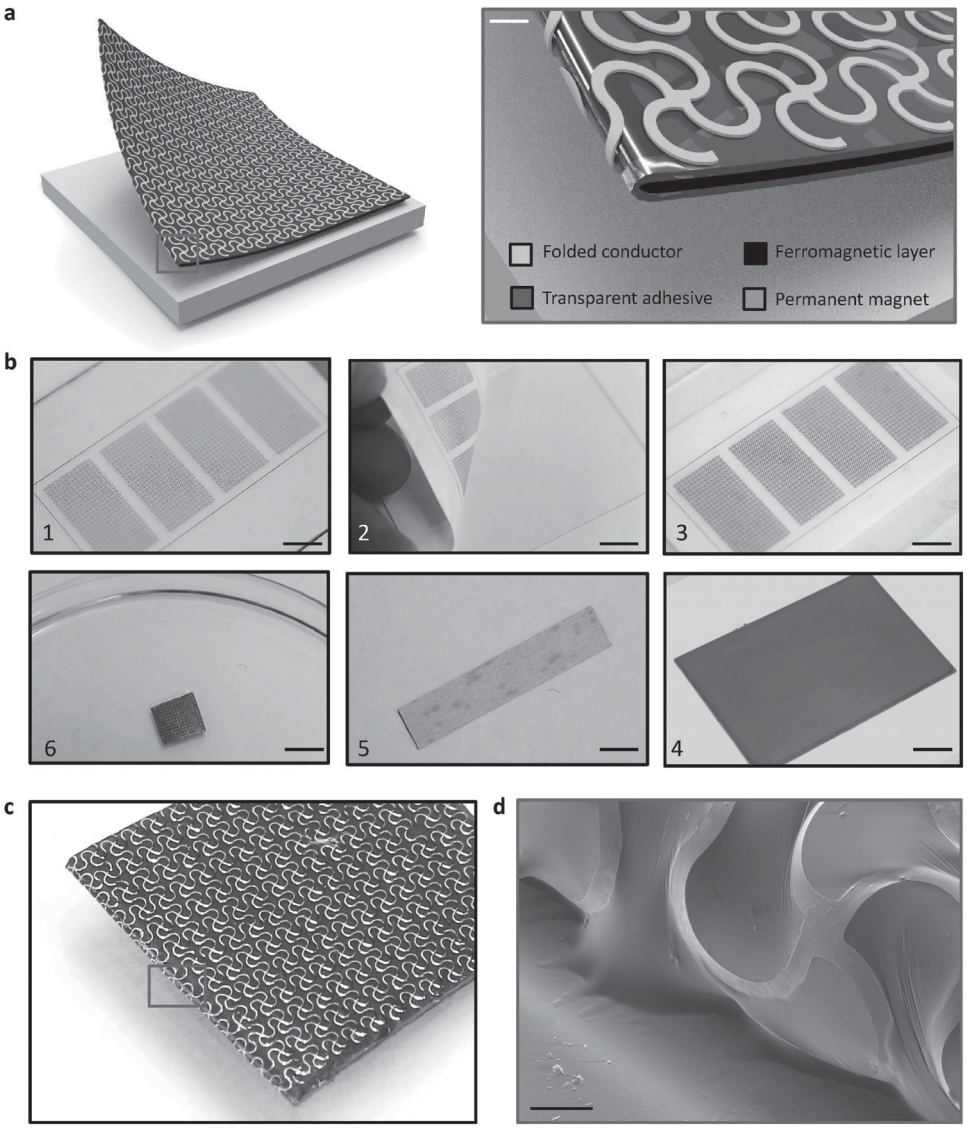

Figure 1. Ferromagnetic, folded, soft electrode composite. a) Schematic diagram of the electrode design and its magnified view. b) Fabrication procedure; scale bar is 1 cm. c) An optical image and scanning electron microscope (SEM) image of fabricated electrode; scale bar is 100 μm.

particles. With this strong magnetic interaction, as shown in Figure 2d, the fabricated electrode composite exhibits 10 times higher adhesion to the magnet (or device direction) than that of the skin.[29–31] Measurements of adhesion strength involve a peeling mode with a force gauge (Mark-10, USA). Each reported result corresponds to an average of measurements on three samples.

As depicted in Figure 2e,f, this type of magnetic stretchable electrode, unlike conventional hydrogel electrodes, retains its original weight when exposed to different levels of humidity. The dimensional instability of the hydrogel adversely affects adhesion strength, contact area, electrical impedance to the skin, and it leads to unpredictable sensor performance.

The soft mechanics is critically important for an intimate, non-irritating interface to the skin. Figure 2g summarizes results of measurements of the elastic modulus of ferromagnetic composite formulations with different volume fractions of CI particles. As the volume fraction increases, the resulting elastic modulus also increases, as might be expected. At the continuum level, the stiffness of a composite depends on some weighted combination of the stiffnesses of the individual constituent materials.[32] The experiments are, in fact, consistent with the Einstein theoretical model of the effective Young's modulus of particle-filled solids, shown by the dotted green line. This model is simply: $G = G_0(1 + 2.5\Phi)$, where G and G_0 are the elastic moduli of a composite and a pure elastomeric material without particles and Φ is the volume fraction.[33,34] As an electrode, lower modulus is desirable to provide free deformation and conformal contact with the skin. At the same time, the electrode must offer sufficiently strong magnetic interaction to the magnet for secure integration. A balance of these considerations led to our choice of 0.1 volume fraction, which yields a material with modulus comparable to the skin ($E \approx 130$ kPa) and an attractive force of interaction with the magnet that is

© 2016 WILEY-VCH Verlag GmbH & Co. KGaA, Weinheim

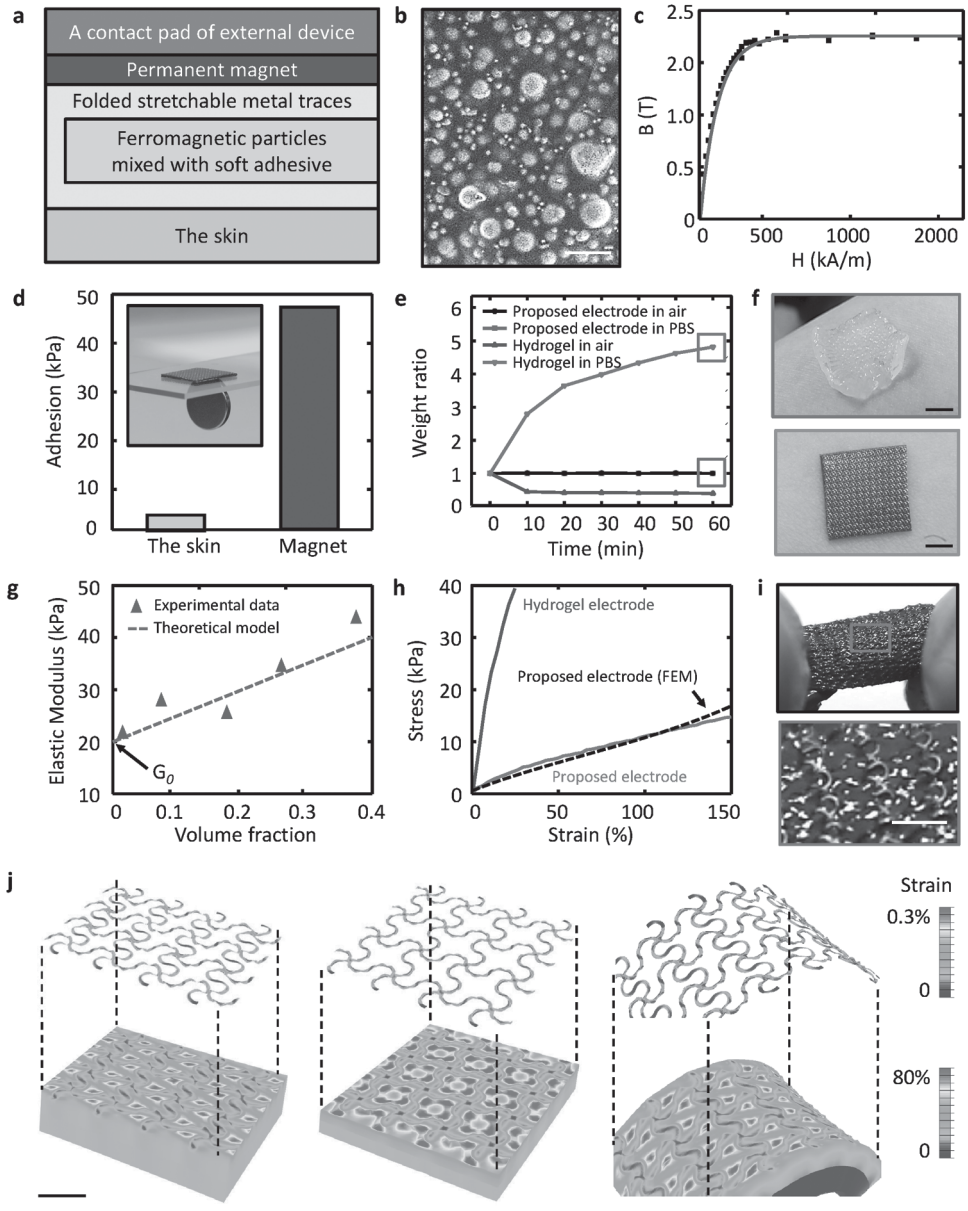

Figure 2. Physical properties of the electrode composite. a) Information on the structure of the composite and its interface with the skin and the contact pad of the external (or wearable) device. b) SEM image of ferromagnetic (carbonyl iron) particles in an elastomer matrix; scale bar is 4 μm. c) Magnetization curve of carbonyl iron powder. d) Comparison of adhesion strength of the electrode composite to the skin and the magnet. Inset: image of the ferromagnetic properties of the electrode composite. e,f) Effect of hydration on the proposed composite and on a commercially available hydrogel electrode. g) Elastic modulus as a function of volume fraction of CI particles in the ferromagnetic composite. h) Mechanical responses of the composite and a commercial hydrogel to applied strain. i) Optical image of the electrode composite under stretching; scale bar is 1 mm. j) Finite-element study for uniaxial stretching (left), biaxial stretching (center), and folding (right); scale bars are 1 mm.

significantly higher than that associated with adhesion to the skin.

As plotted in Figure 2h,i, the full electrode structure also has a low modulus, elastic behavior under large strain deformation. The total stretchability (more than 150%) and skin-like modulus ($E \approx 40$ kPa) are key characteristics. Figure 2j–l shows the deformed shapes and distributions of strain determined by 3D finite-element analysis under uniaxial/biaxial stretching and bending. The serpentine design leads to strains in the electrode materials that are ≈2 orders of magnitude smaller than those in the elastomers. The uniaxial/biaxial elastic stretchability and bendability are 25%, 24%, and 0.46 mm^{-1}, respectively, for ≈0.3% yield strain of Au.

Accurate and reliable recording of EP signals benefits from low impedance, temporally stable contacts to the skin. As a summary of results, **Figure 3**a–h presents the measured impedance to the skin for various parameters: electrode type, filling factor, skin hydration, and frequency. The measurements involve a pair of identical electrodes (contact area = 1 cm by 1 cm; distance between two electrodes = 5 cm) laminated on the

© 2016 WILEY-VCH Verlag GmbH & Co. KGaA, Weinheim

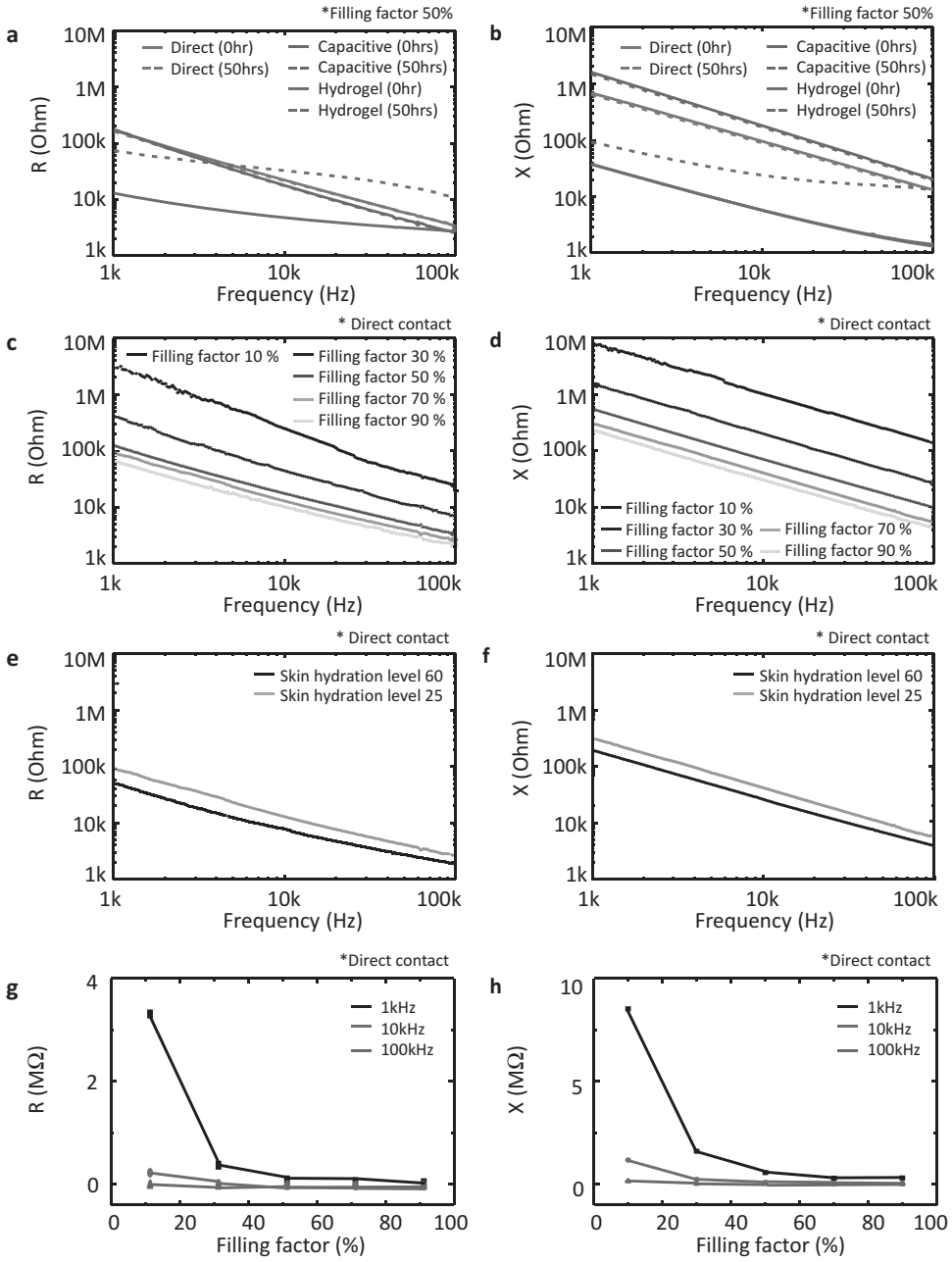

Figure 3. Impedance measurements associated with contact between the electrodes and the skin. a,b) Type of contact: direct, capacitive, and hydrogel. c,d) Filling factor of direct contact area to entire electrode, e,f) skin hydration level, and g,h) frequency. Dotted lines present fitted curves to the measured data.

flexor carpi radialis of the forearm. Figure 3a,b presents results for different types of electrodes. The commercial hydrogel electrode exhibits lower impedance than direct or capacitive magnetic stretchable electrodes (measured with comparable overall areas, rather than just electrical interface areas) but its impedance significantly increases after 50 h due to effects of shrinkage and evaporative drying while that of the other electrodes remains constant. The magnetic stretchable electrodes have impedances that depend on filling factor (active sensing component, as defined by the area of the serpentine structure, to total electrode area), skin hydration level, and frequency. The impedances show a linear dependence on frequency in log–log scale as shown in Figure 3c–f, and an inverse dependence on filling factor in linear–linear scale as shown in Figure 3g,h. A simple equivalent circuit model yields some insights. As in **Figure 4**a, the electrodes lie between the electrical lead-out (or thin magnet bonded on contact pad) and the skin (or epidermis). The associated model is in Figure 4b.[35,36] Here, the voltage source E_{hc} corresponds to the half-cell potential, the capacitance C_d indicates the electrical charge accumulated between the electrode and the skin, R_d is the resistance between the electrode and the skin during the charge transfer, and R_s

© 2016 WILEY-VCH Verlag GmbH & Co. KGaA, Weinheim

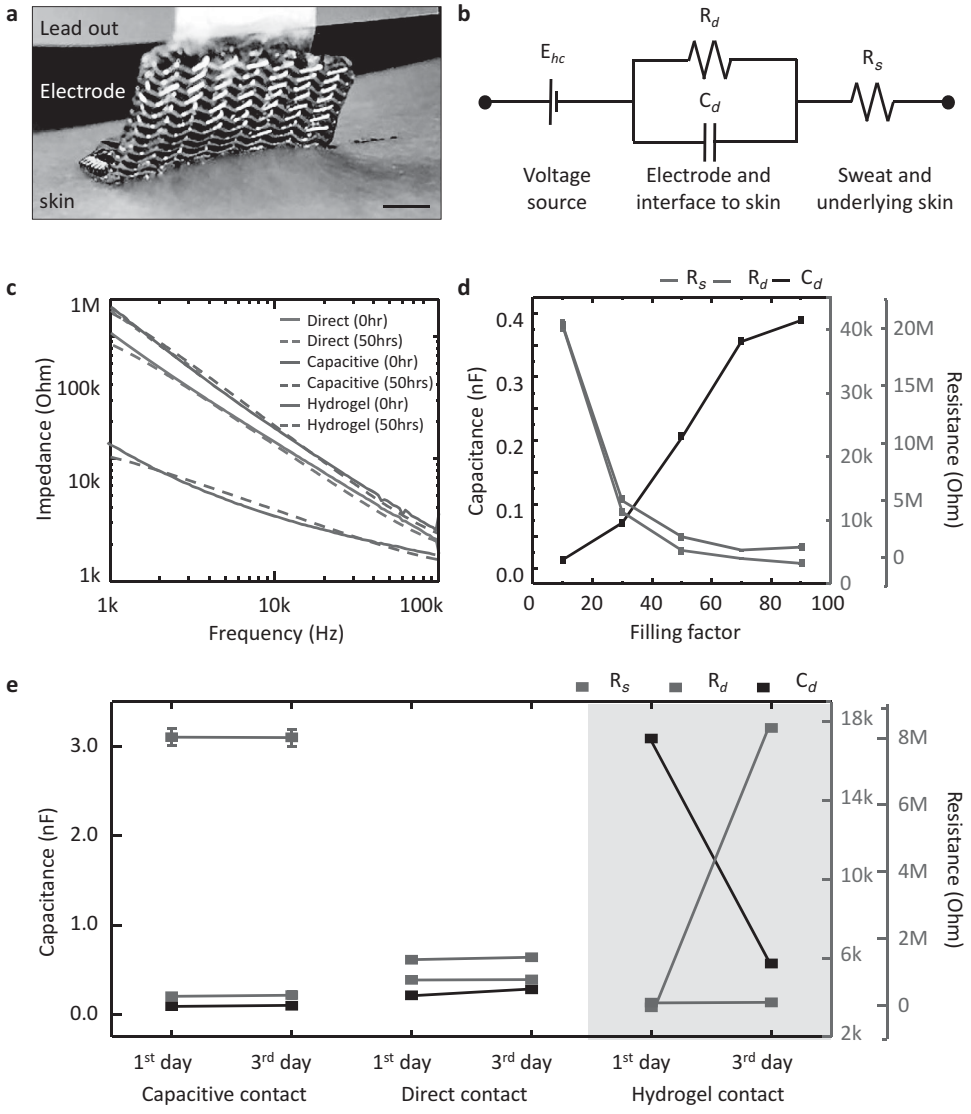

Figure 4. Impedance analysis with equivalent circuit model. a) Optical image of electrode system on the skin, and b) equivalent circuit model. c) Measured impedance data and their fitted curve. d) Extracted parameters according to filling factor, and e) type of electrode and elapsed time.

is related to the sweat and the underlying skin tissue, such as epidermis, dermis, and subcutaneous layers. The resistance of the sweat and underlying skin tissue (R_s) should be in series with R_d and C_d. In this model, the electrochemical impedance, current variance caused by sinusoidal potential perturbation, is simplified by two components of the charge transfer (faradaic current) and double layer capacitance on the surface of the electrode. The resistance in sweat and tissue affects the total impedance since both the charge transfer and capacitance depends on the solution resistance, R_s. However, R_s, alone itself, cannot be an independent current path. In this study, we chose the equivalent circuit model from Oliveira et al.[35] This model is the most simplified version to describe electrochemical impedance of the electrode in electrolyte. The reference has similar geometrical configuration and resulting electrical impedance of their electrode to those of our electrode. As in Figure 4c, fits to the data (Levenberg–Marquadt algorithm) yield values for the key parametrs. In Figure 4d, as the areal filling factor increases, the capacitance also increases but both resistances decrease. This analysis indicates that larger active sensing areas provide higher capacitances and lower resistances, as might be expected. As presented in Figure 4e, the model parameters remain constant over several days, in contrast to those for hydrogel electrodes. A commercially available hydrogel electrode (AG735, Axelgaard Manufacturing, USA) provides a useful point of comparison. As shown in Figure 4e, the fitted R_d, C_d, and R_s values of the hydrogel electrode with the circuit model are 0.12 Mohm, 0.2 nF, 3.1 kohm, consistent with previous reports (R_d, = 0.1–1 Mohm, C_d = 0.1–10 nF, and R_s = 0.1–10 kohm).[37,38] These parameters, of course, depend on the geometries of the electrodes and the chemical composition of the hydrogel.

Figure 5a,b presents a schematic diagram and an optical image of these electrodes integrated with a thin, stretchable recording platform with wireless operation (BiostampRC, MC10, Inc). Each electrode mounts to a thin permanent

© 2016 WILEY-VCH Verlag GmbH & Co. KGaA, Weinheim

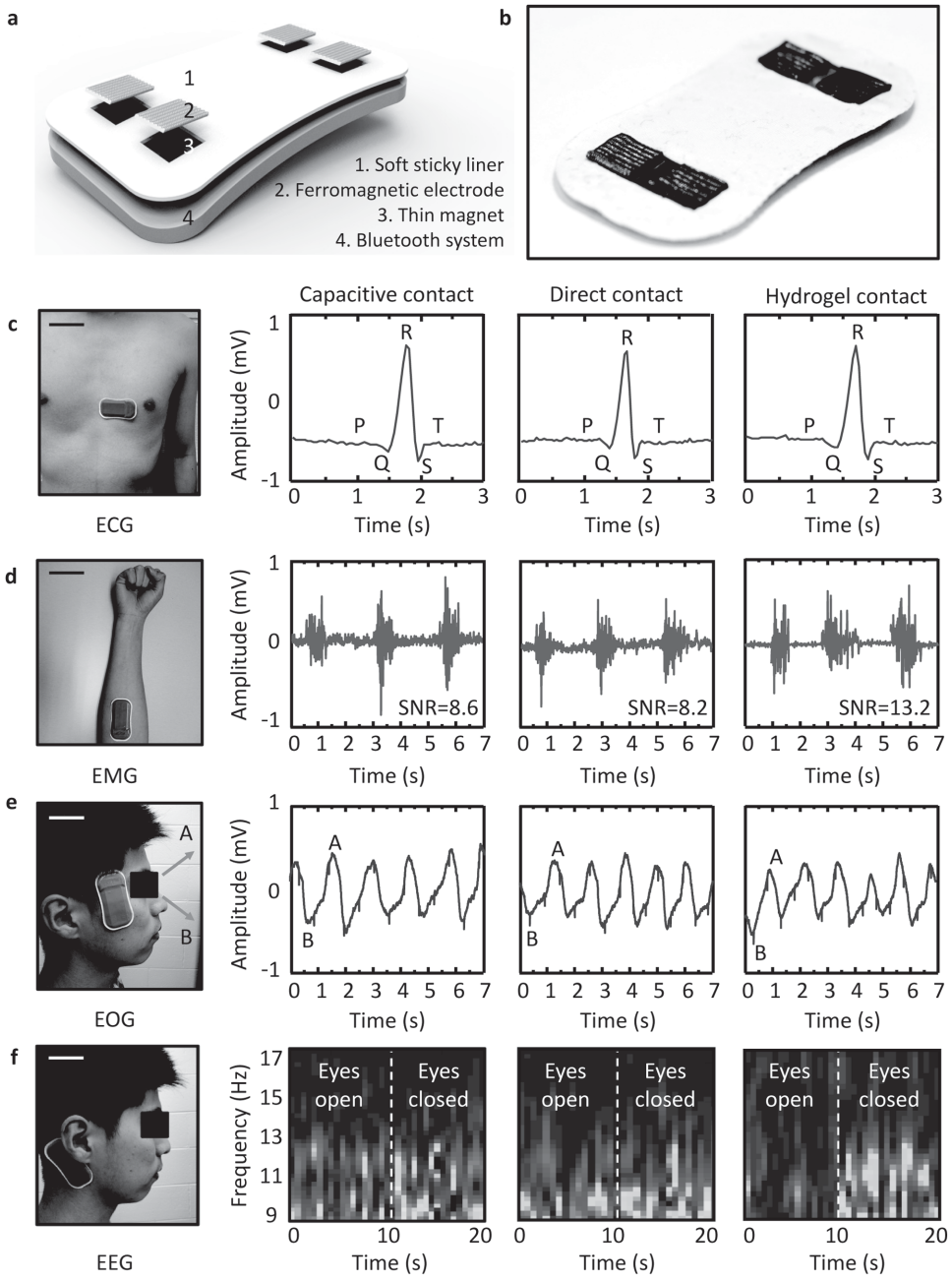

Figure 5. Device-level integration of the proposed electrode composite. a) Schematic illustrations and b) optical images of wireless electrophysiology (EP) monitoring systems integrated with soft, folded magnetic electrode composites. Optical images of the device on the body and associated captured EP data: c) electrocardiogram (ECG), d) electromyogram (EMG), e) electrooculogram (EOG), and f) electroencephalogram (EEG). Scare bars are 10 cm in (c,d) and 5 cm (e,f).

magnet (NdFeB) with a force that provides reliable electrical contact and mechanical coupling. A conductive epoxy (CircuitWorks, CW2400, USA) bonds the magnets to solid metal pads on the BiostampRC, with negligible resistance (<0.001 ohm-cm). The shell elastomer serves as a soft adhesive (*Silbione* Firm Gel, Bluestar Silicones, France, $E \approx 20$ kPa) to the skin. In this way, various EP signals, including electrocardiogram (ECG), electromyogram (EMG), electroocoloculogram (EOG), and electrocepharlogram (EEG) can be captured and stored locally in the BiostampRC memory module or continuously transmitted to an external receiver via a Bluetooth protocol. In these experiments, we used two different BiostampRC devices. Compared to the device for capacitive contact, the other one for hydrogel and direct contact is designed to have a compensative capacitor to analog front end of the device. With this target-oriented circuit modification, EP signals are successfully collected. Figure 5c–f summarizes results of various experiments. As a first example, ECG signals

© 2016 WILEY-VCH Verlag GmbH & Co. KGaA, Weinheim

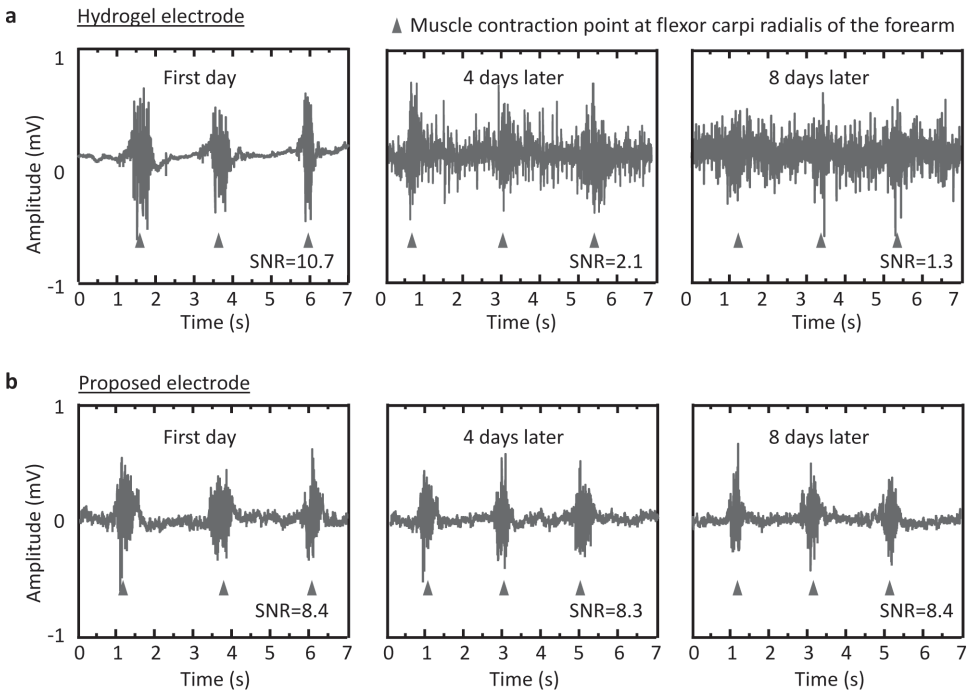

Figure 6. Long-term usability with wireless EMG recording. Data captured using a) a hydrogel electrode and b) soft, folded magnetic electrode. Each red triangle indicates a specific point of muscle contraction of the flexor carpi radialis of the forearm.

acquired with both capacitive- and direct contact electrodes from the chest show clearly the *P* wave, the QRS complex, and the *T* wave with a quality of measurement that is comparable to that of data using hydrogel electrode. EMG signals captured from the flexor carpi radialis of the forearm show similarly high quality. In this case, the signal-to-noise ratio (SNR) ranges from 8.2 to 13, suitable for use in both clinical applications and human–machine interfaces (HMI).[9,39] Placing the device near the left or right eyes allows recording of EOG signals. The experiments involved data collection while the subject moved his eyes up and down. As can be seen in Figure 5e, the data capture eye movement accurately, with potential for use in ophthalmological diagnosis in training procedures and in human–machine interfaces. As a last example, EEG signal collected with a device on the mastoid clearly shows alpha rhythms with frequencies between 8 and 12 Hz when the eyes are closed, of potential relevance in cognitive state monitoring and brain computer interfaces.[39]

A series of experiments of wireless EMG monitoring highlight long-term usability of the system. As in **Figure 6**, the quality of EMG signal from the flexor carpi radialis of the forearm recorded with a hydrogel electrode degrade quickly due to unavoidable evaporation of water. The signals and their SNR value captured using these dry, soft magnetic electrodes maintain their original quality. The limit of detection of their electromyogram are ≈0.05 mV for capacitive contact electrode, ≈0.04 mV for direct contact electrode, 0.01 mV for fresh hydrogel contact electrode, and 0.5 mV for dried (8 d later) hydrogel contact electrode in room temperature and atmosphere. In this case, the sensitivity levels, which means EMG response amplitude for almost same muscle groups for similar activities are similar for each case.

3. Conclusion

The materials, designs, and integration strategies presented here provide a framework for ferromagnetic, folded, soft electrodes with capabilities in long-term use and system-level integration in EP monitoring. The main advantages of this system are in 1) intimate and persistent contact to the skin, without irritation, 2) dimensionally stable, engineered designs for robust adhesion and electrical measurement interfaces to the skin, and 3) direct and reversible bonding to external wireless recording/transmission electronics by magnetic force. As an advanced form of epidermal electronics, these design schemes are fully compatible with the most sophisticated EP monitoring system that are commercially available. These same concepts can apply to many other types of epidermal electronics with various other measurement modalities, including those that involve thermal, mechanical, and chemical sensing.

4. Experimental Section

Fabrication of the Electrode Composite: Polymethylmethacrylate (PMMA, 100 nm) coated on a glass slide ($70 \times 50 \times 1.0$ mm^3) served as a sacrificial layer to facilitate release. Spin casting and thermal curing (2 h at 250 °C in a vacuum oven) a film of polyimide (PI; 2 μm in thickness, HD Microsystems, USA) yielded an overcoat on the PMMA. Photolithographic patterning of bi-layers of Cr (10 nm)/Au (200 μm) formed by electron beam evaporation (AJA International, USA) defined the conductive elements of the mesh. Reactive ion etching (50 mTorr, 40 sccm CF4, and 100 W for 10 min) of the exposed PI created an open architecture layout to provide mechanical stretchability and exposed regions to

© 2016 WILEY-VCH Verlag GmbH & Co. KGaA, Weinheim

facilitate adhesion to the skin. Undercutting removed the PMMA layer to allow release onto a water-soluble tape (Aquasol, USA) for subsequent integration with a pre-strained compliant and sticky elastomeric substrate (*Silbione* Firm Gel, Bluestar Silicones, France, $E \approx 20$ kPa). Spin-casting a layer of *silbione* and a layer of soft adhesive formed by mixing carbonyl iron powder with uncured *silbione* at a 1:9 ratio by volume, formed a bilayer on the surface of the tape. Partially curing these materials by heating to 70 °C in an oven for 10 h, folding electrode in half and then completing the cure by continued baking for 24 h completed the fabrication. Dissolving the water-soluble tape by dipping the samples into water and drying them at room temperature and atmosphere prepared the electrodes for integration with the recording apparatus and the skin.

Measurements of Magnetization: The magnetization curves of the electrode composite were determined with a superconducting quantum interference device magnetometer (S600X SQUID susceptometer, UK).

Measurements of Stress–Strain Responses: Mechanical properties of all samples were measured with a dynamic mechanical analyzer (DMA; TA instruments, Q800). Characterizing the applied force versus the displacement under uniaxial tensile loading at room temperature yielded data for determination of the mechanical modulus. Each of the reported results corresponds to an average of measurements on three samples.

Finite-Element Analysis: ABAQUS commercial software[40] was used to study the mechanics of a mesh electrode [200 nm thick Au (elastic modulus 80 GPa and Poisson's ratio 0.44)/1.2 μm thick PI (elastic modulus 2.5 GPa and Poisson's ratio 0.34)] on a bi-layer substrate [0.5 mm thick layer of silbione (elastic modulus ≈20 kPa and Poisson's ratio 0.5)/0.5 mm thick ferromagnetic layer (elastic modulus ≈30 kPa and Poisson's ratio 0.5)]. Eight-node 3D solid elements and four-node shell elements were used for the bi-layer substrate and electrode, respectively, with refined meshes to ensure the accuracy.

Measurement of Electrical Impedance: Quantitative analysis of electrical impedances between the stretchable magnetic electrodes and the skin over a frequency range of 1–100 kHz was performed with a precision LCR meter (Agilent, E4980A, USA).

Device-Level Integration of the Stretchable Magnetic Electrodes: Bonding and room temperature curing of thin (2 mm) permanent magnets (NdFeB) onto contact pads of on a BiostampRC monitoring system utilized a conductive epoxy (CircuitWorks, CW2400, USA). Assembling the electrode composites onto the magnets relied on magnetic interactions between these two components. An adhesive, fabric liner bonded the non-electrode regions of the BiostampRC platform to the skin.

Experiments on Human Subjects: All experiments on human skin were conducted under approval from Institutional Review Board at the University of Illinois at Urbana-Champaign (protocol number: 13229).

Acknowledgements

K.-I.J. and H.N.J. contributed equally to this work. This work used facilities in the Frederick Seitz Materials Research Laboratory and the Center for Microanalysis of Materials at the University of Illinois at Urbana-Champaign. Y.M. and X.F. acknowledge the support from the National Basic Research Program of China (Grant No. 2015CB351900) and National Natural Science Foundation of China (Grant Nos. 11402135 and 11320101001). Y.H. acknowledges the support from NSF (DMR-1121262, CMMI-1300846, and CMMI-1400169) and the NIH (Grant No. R01EB019337). The middle name of B. H. Kim was updated on October 25, 2016, after initial publication on early view.

Received: June 22, 2016
Revised: August 10, 2016
Published online: September 9, 2016

[1] Y. M. Chi, T.-P. Jung, G. Cauwenberghs, *IEEE Rev. Biomed. Eng.* **2010**, *3*, 106.
[2] A. C. Myers, H. Huang, Y. Zhu, *RSC Adv.* **2015**, *5*, 11627.
[3] W. D. Hairston, K. W. Whitaker, A. J. Ries, J. M. Vettel, J. C. Bradford, S. E. Kerick, K. McDowell, *J. Neural Eng.* **2014**, *11*, 046018.
[4] A. Searle, L. Kirkup, *Physiol. Meas.* **2000**, *21*, 271.
[5] S. C. Mukhopadhyay, *Wearable Electronics Sensors for Safe and Healthy Living*, Springer, Switzerland **2015**.
[6] J. A. Rogers, R. Ghaffari, D.-H. Kim, *Stretchable Bioelectronics for Medical Devices and Systems*, Springer, Switzerland **2016**.
[7] D. H. Kim, N. S. Lu, R. Ma, Y. S. Kim, R. H. Kim, S. D. Wang, J. Wu, S. M. Won, H. Tao, A. Islam, K. J. Yu, T. I. Kim, R. Chowdhury, M. Ying, L. Z. Xu, M. Li, H. J. Chung, H. Keum, M. McCormick, P. Liu, Y. W. Zhang, F. G. Omenetto, Y. G. Huang, T. Coleman, J. A. Rogers, *Science* **2011**, *333*, 838.
[8] S. Smith, *J. Neurol. Neurosurg. Psychiatry* **2005**, *76*, ii2.
[9] J. W. Jeong, W. H. Yeo, A. Akhtar, J. J. S. Norton, Y. J. Kwack, S. Li, S. Y. Jung, Y. W. Su, W. Lee, J. Xia, H. Y. Cheng, Y. G. Huang, W. S. Choi, T. Bretl, J. A. Rogers, *Adv. Mater.* **2013**, *25*, 6839.
[10] J. du Plessis, A. Stefaniak, F. Eloff, S. John, T. Agner, T. C. Chou, R. Nixon, M. Steiner, A. Franken, I. Kudla, L. Holness, *Skin Res. Technol.* **2013**, *19*, 265.
[11] C. Blichmann, J. Serup, *Contact Dermatitis* **1987**, *16*, 155.
[12] X. Huang, W. H. Yeo, Y. H. Liu, J. A. Rogers, *Biointerphases* **2012**, *7*, 52.
[13] W. H. Yeo, Y. S. Kim, J. Lee, A. Ameen, L. K. Shi, M. Li, S. D. Wang, R. Ma, S. H. Jin, Z. Kang, Y. G. Huang, J. A. Rogers, *Adv. Mater.* **2013**, *25*, 2773.
[14] S. X. Yang, Y. C. Chen, L. Nicolini, P. Pasupathy, J. Sacks, B. Su, R. Yang, D. Sanchez, Y. F. Chang, P. L. Wang, D. Schnyer, D. Neikirk, N. S. Lu, *Adv. Mater.* **2015**, *27*, 6423.
[15] T. Igarashi, L. Nishino, S. K. Nayar, *The Appearance of Human Skin: A Survey*, Now Publishers Inc., New York **2007**.
[16] J. W. Jeong, M. K. Kim, H. Y. Cheng, W. H. Yeo, X. Huang, Y. H. Liu, Y. H. Zhang, Y. G. Huang, J. A. Rogers, *Adv. Healthcare Mater.* **2014**, *3*, 642.
[17] E. Calo, V. V. Khutory anskil, *Eur. Polym. J.* **2015**, *65*, 252.
[18] N. A. Alba, R. J. Sclabassi, M. G. Sun, X. T. Cui, *IEEE Trans. Neural Syst. Rehabil. Eng.* **2010**, *18*, 415.
[19] A. Myers, L. Du, H. Huang, Y. Zhu, *IEEE Engineering in Medicine and Biology Society Conf. Proc.* (Ed: Z.-P. Liang), IEEE, **2014**, p. 1.
[20] A. Myers, L. Du, H. Huang, Y. Zhu, *RSC Adv.* **2015**, *5*, 11627.
[21] S. M. Lee, H. J. Byeon, J. H. Lee, D. H. Baek, K. H. Lee, J. S. Hong, S.-H. Lee, *Sci. Rep.* **2014**, *4*, 6074.
[22] M. K. Yapici, A. A. Tamador, Y. A. Samad, K. Liao, *Sensors Actuat. B-Chem.* **2015**, *221*, 1469.
[23] H. C. Jung, J. H. Moon, D. H. Baek, J. H. Lee, Y. Y. Choi, J. S. Hong, S.-H. Lee, *IEEE Trans. Bio.-Med. Eng.* **2012**, *59*, 1472.
[24] J. H. Lee, Y. W. Nam, H. C. Jung, D. H. Baek, S. H. Lee, J. S. Hong, *Biochip J.* **2012**, *6*, 91.
[25] M. A. Abshinova, L. Kuritka, N. E. Kazantseva, J. Vilcakova, P. Saha, *Mater. Chem. Phys.* **2008**, *114*, 78.
[26] V. G. Syrkin, S. Tolmasskii, A. A. Petrova, *Sov. Powder Metall.* **1966**, *5*, 545.
[27] F. N. D. Neto, O. A. Araujo, L. R. Guilherme, V. K. Garg, A. C. Oliveira, P. E. N. de Souza, A. Franco, *Mater. Chem. Phys.* **2015**, *162*, 100.
[28] I. Bica, *J. Ind. Eng. Chem.* **2009**, *15*, 605.
[29] R. M. Jolly, J. D. Carlson, B. C. Munoz, *Smart Mater. Struct.* **1996**, *5*, 607.

© 2016 WILEY-VCH Verlag GmbH & Co. KGaA, Weinheim

[30] K.-I. Jang, J. Seok, B.-K. Min, S. J. Lee, *J. Magn. Magn. Mater.* **2009**, *321*, 1167.
[31] C. Bellan, G. Bossis, *Int. J. Mod. Phys. B* **2002**, *16*, 2447.
[32] S. B. Jörgen, C. B. Mary, *Rubber Chem. Technol.* **1999**, *72*, 633.
[33] A. Einstein, *Ann. Phys.* **1906**, *19*, 229.
[34] H. M. Smallwood, *J. Appl. Phys.* **1944**, *15*, 758.
[35] C. C. Oliveira, J. M. de Silva, I. G. Trindade, F. Martines, *Conf. Design of Circuits and Integrated Circuits* (Ed: T. Riesgo, J. Uceda), IEEE, **2014**, p. 1.
[36] N. Meziane, J. G. Webster, M. Attari, A. J. Nimunkar, *Physiol. Meas.* **2013**, *34*, R47.
[37] A. Albulbul, A. D. C. Chan, *IEEE Int. Symp. Medical Measurements and Applications Proc.* (Ed: V. Groza), IEEE, **2012**, p. 1.
[38] B. Taji, S. Shirmohammadi, V. Groza, I. Batkin, *IEEE Trans. Instrum. Meas.* **2014**, *63*, 1412.
[39] L. F. Nicholas-Alonso, J. Gomez-Gil, *Sensors* **2012**, *12*, 1211.
[40] ABAQUS Analysis User's Manual **2010**, V6.10.

© 2016 WILEY-VCH Verlag GmbH & Co. KGaA, Weinheim